Metallography, Microstructure, and Analysis (2020) 9:660–667
https://doi.org/10.1007/s13632-020-00680-z

TECHNICAL ARTICLE

Structural Study of Undeformed and Deformed Maraging C300 Steels Using X-ray Diffraction Measurements

Ricardo Vilain de Melo[1] · Carlos Augusto Silva de Oliveira[1] · Claudio Michel Poffo[2] · Hamilton Ferreira Gomes de Abreu[3]

Received: 30 June 2020 / Revised: 31 August 2020 / Accepted: 3 September 2020 / Published online: 28 September 2020

Abstract
A high Ti content maraging C300 steel was analyzed by X-ray diffraction measurements to study the effect of aging at 773 K for different treatment times by monitoring lattice parameter, microstrain, crystallite size and formation/dissolution of intermetallic Ni_3(Ti, Mo). The results showed a strong influence of cold and hot deformation over precipitation of the coherent metastable orthorhombic phase Ni_3(Ti, Mo). The volumetric fraction of this precipitation can go up to 14 and 19% in non-deformed and deformed samples, respectively. At longer aging time, this precipitate starts to dissolve to form a more stable μ phase and reverse austenite. Also, the results showed a strong influence of deformation and precipitation on crystallite size and microstrain.

Keywords X-ray diffraction · Hot/cold deformation · Precipitation · Maraging steel · Williamson–Hall

Introduction

Precipitate and reverse austenite formation, as well as their effects on the properties of maraging steels during aging at temperatures above 723 K, with and without deformation, have been studied in recent years [1–9]. The growing interest in maraging steels is due to their ultra-high strength combined with good toughness. This ultra-high strength is the result of homogeneous precipitation of Ti- and Mo-based nanometric intermetallic in a low-carbon martensitic matrix. These characteristics make possible the use of these steels by military, aerospace and nuclear industry in components that require high reliability [10–14].

In order to reach their final properties, maraging steels are, usually, solubilized between 1093 and 1373 K [10, 15–20] and then aged for intermetallic precipitation between 673 and 873 K [8, 14, 21–23]. The mechanical strength of these steels can also be increased by cold and/or hot plastic deformation, which leads to a reduction in toughness and the increase in precipitation and reverse austenite formation kinetics [2, 7–9]. The effect of deformation on precipitation occurs due to the increased density of dislocation present in the material, accelerating atomic diffusion and, consequently, accelerating the formation of solute clusters and precipitation [8]. This increase in atomic diffusion also leads to a faster rate of precipitate growth, allowing a faster local enrichment of Ni and Mo, that leads to an acceleration of reverse austenite formation [9, 24, 25].

However, although there is a lot of work in the literature about maraging steels, there are also several differences in them. One example is the crystalline structure of the martensitic matrix, which is historically cited as body-centered cubic (BCC) [2, 12, 26–29], but recent articles show that strong saturation of substitutional elements causes tetragonal distortion in this matrix [5, 6, 15, 30]. Another difficulty found in the literature is the quantification of precipitates. Some studies using Monte Carlo simulation [31], phase transformation theories

✉ Ricardo Vilain de Melo
vilainricardo@gmail.com

Carlos Augusto Silva de Oliveira
carlos.a@ufsc.br

Claudio Michel Poffo
claudio.poffo@ufsc.br

Hamilton Ferreira Gomes de Abreu
hamilton@ufc.br

[1] Departamento de Engenharia Mecânica, Universidade Federal de Santa Catarina, Florianópolis, Brazil

[2] Coordenadoria Especial de Engenharia de Materiais, Universidade Federal de Santa Catarina, Blumenau, Brazil

[3] Departamento de Engenharia Metalúrgica e de Materiais, Universidade Federal do Ceará, Fortaleza, Brazil

[32, 33] and DSC curves [34] have quantified the precipitation in maraging steel, but generally count all precipitates in the same theory and/or simulating upon a phase equilibrium condition.

It is well known that the main reason for the increase in the mechanical resistance of maraging steel is the metastable precipitates, listed in the literature as: Ni_3Ti [2, 10, 16, 26, 35], Ni_3Mo [21, 36–38] and/or Ni_3 (Ti, Mo) [39, 40]. The formation of these occurs in the first seconds of aging, and with increasing aging time, they grow and dissolve forming incoherent Fe_2Mo [21, 36, 41] and/or Fe_7Mo_6 [36, 42] precipitates, beside reverse austenite.

Traditionally, in maraging steels, the XRD technique is used to quantify reverse austenite using temperatures higher than 823 K at times ranging from a few minutes to tens of hours [2, 8–10, 29, 43]. As the increase in the aging temperature leads to an increase in the formation of stable precipitates and reversed austenite, a reduction in the fraction of metastable precipitates and an acceleration in their dissolution, at temperatures higher than 823 K it is difficult to distinguish metastable precipitates in X-ray diffraction. In addition to phase formation, the X-ray diffraction also enables to verify the influence of deformation on crystallite size, microstrain and lattice parameter [44].

In order to understand the precipitation kinetics in maraging steels and its correlation with aging time and deformation, this work was carried out a study via XRD measurements in a high Ti content maraging C300 steel aged at 773 K with aging times up to 200 h with and without prior hot and cold deformation. This work also evaluated the influence of theses variations on matrix lattice parameters and microstrain, crystallite size and intermetallic formation/dissolution.

Methodology

This work studied a high Ti content maraging C300 steel with chemical composition given in Table 1. It analyzed 12 different experimental diffractions pattern obtained by a Philips X 'Pert Pro diffractometer using a Co $K\alpha$ radiation source ($\lambda = 1.7998$ Å). The intensity measurements were performed with a 0.02° step in the $30° < 2\theta < 120°$ range. The conditions studied were: without deformation (WD), hot forged (HF) and hot and cold rolled (CR). All XRD patterns were refined using the Rietveld method [45] implemented in the GSAS package [46]. In order to subtract the instrumental broadening, the XRD pattern of a certified elemental silicon sample was used for the Rietveld refinements.

To obtain the WD and HF conditions, 8 cubic samples were machined with 10 mm edge from a cylinder of radius 170 mm and 10 mm high. All the 8 samples were heated at 1323 K for 1 h. Sequentially, 4 of 8 those samples (WD condition) were water-quenched. The remaining 4 samples were hot-forged at 1323 K with a 50% reduction in height and readily water-quenched (HF condition). For the manufacture of the CR condition, it was machined a 100×50×20 mm parallelepiped from a cylinder of radius 170 mm and 20 mm high, that had, sequentially, a 50% height reduction by hot rolling at 1473 K followed by water quench. The result plate had a further 50% reduction in height by cold rolling at room temperature, from where 4 samples with dimensions of 10x10x5 mm were taken.

For each deformation condition, 4 samples were aged at 773 K, each for a distinct time period: 0, 10, 50 and 200 h. All samples were embedded in polyester resin, ground and polished with 1 µm diamond paste before being analyzed by X-ray diffraction. For this, the Rietveld method was used using the GSAS software, where correlated the experimental peaks with the space groups I4 [5], Fm-3m (ICDS 632930), PmmnZ (ICDS 644046) and R-3H (ICDS 632623) for the martensite, austenite, Ni_3(Ti, Mo) and µ phases, respectively.

To study the influence of deformation and aging over the samples, it evaluated the variation in the width of the peaks obtained by the XRD measurements. Assuming that the correlation between the full width at half maximum (FWHM) and the diffraction angle is of monotonic type, it is possible to quantify the average size of the crystallite, D, and the average microstrain, ε, from the pattern of XRD patterns. This quantification is performed by the Williamson–Hall (W–H) equation, Eq 1, where θ is the angle of peak diffraction, Γ the FWHM, λ the X-ray wavelength used, and k a constant usually used as 0.9 [47]. The Γ and θ values are obtained directly from the Rietveld refinement.

$$\Gamma \cos\theta = \frac{k\lambda}{D} + 4\varepsilon \sin\theta \tag{1}$$

W–H analysis assumes that the strain is uniform in all crystallographic directions, thus considering the isotropic nature of the crystal, where the material properties are independent of the direction along which they are measured [47].

Results

Figure 1 shows the variation in the intensity of diffraction peaks as a function of deformation in non-aging samples.

Figures 2, 3 and 4 show the influence of aging at 773 K on the experimental diffraction pattern of WD, HF and CR conditions, respectively, and Table 2 shows the phase

Table 1 Chemical composition of the studied material

Ni	Co	Mo	Ti	Al	C	Mn	Si	Fe
18.6	9.4	5.2	1.0	0.10	0.03	0.04	0.19	Bal

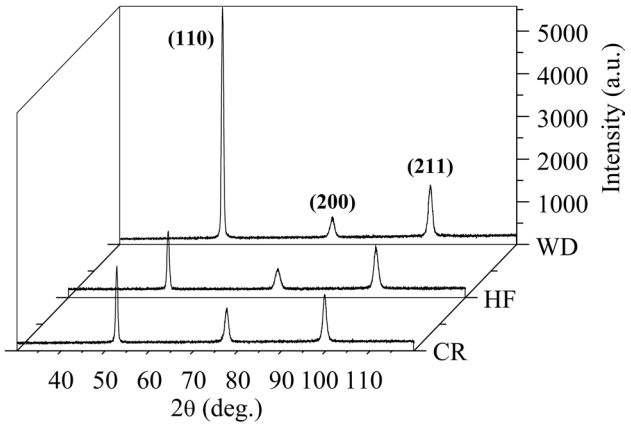

Fig. 1 Experimental diffractions pattern of non-aged samples in the WD, HF and CR conditions

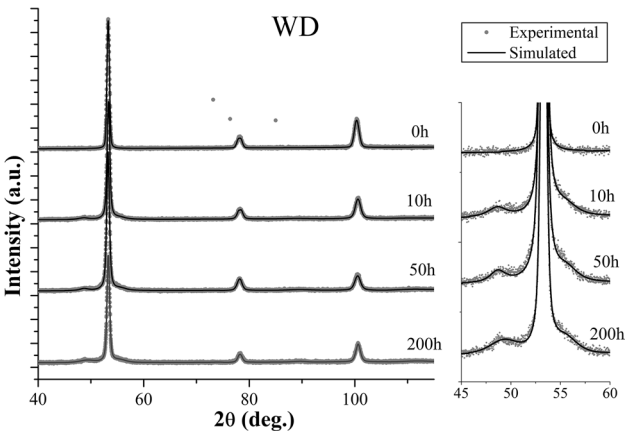

Fig. 2 Experimental diffractions pattern of WD condition aged for 0, 10, 50 and 200 h at 773 K

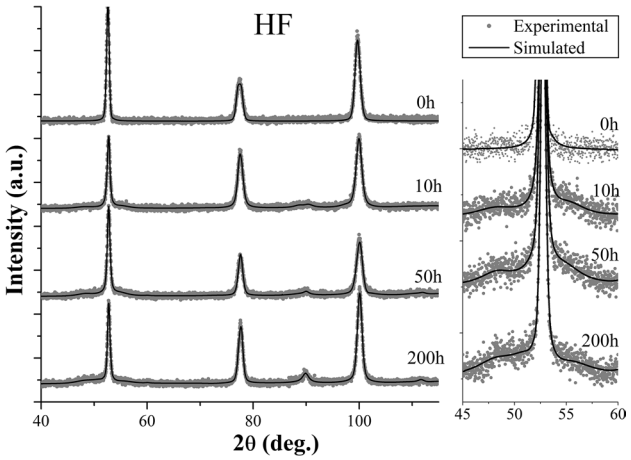

Fig. 3 Experimental diffractions pattern of HF condition aged for 0, 10, 50 and 200 h at 773 K

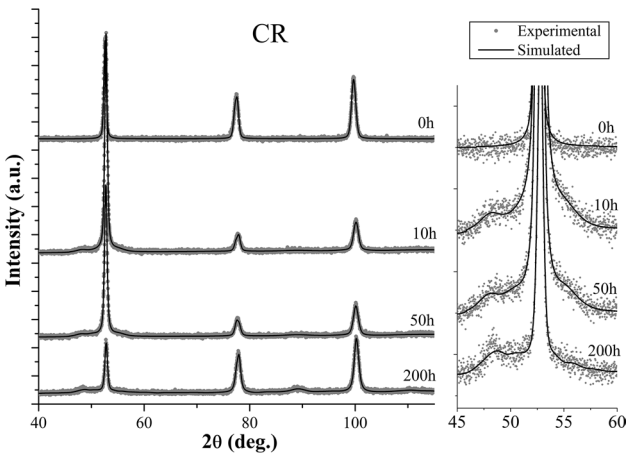

Fig. 4 Experimental diffractions pattern of CR condition aged for 0, 10, 50 and 200 h at 773 K

percentage and lattice parameters, obtained from Rietveld method [45], besides microstrain and crystallite size, calculated by the W–H equation, for the WD, HF and CR conditions, respectively.

After aged for 10 h at 773 K, all conditions showed a lattice parameter reduction of α'. When aged for 50 h, it observed a faster reduction in the HF and CR conditions, while for the WD condition it observed a stabilization of the lattice parameter. When aged for 200 h, the lattice parameter of the HF and CR conditions increased, while that of the WD condition reduced when compared to samples aged for 50 h, as shown in Table 2.

When aged for 10 h, in addition to α', it observed the formation of 10, 13 and 16% Ni_3(Ti, Mo) for WD, HF and CR conditions, respectively. After aged for 50 h, the Ni_3(Ti, Mo) fraction increased to 11, 19, 19% for WD, HF and CR conditions, respectively. In the HF condition, it was possible to find the presence of reverse austenite, γ; however, the low volume fraction precluded its quantification.

After aged for 200 h, the Ni_3(Ti, Mo) fraction decreased under HF and CR conditions to 11 and 17%, respectively, while under WD condition the fraction of Ni_3(Ti, Mo) increased to 14%. With 200 h of aging, it observed the presence of γ in the WD and HF conditions and that of μ phase [48] in the CR condition. However, the low volume fraction observed complicates the quantification of those phases.

The values of ε and D were obtained from the equation of W–H, Eq 1, as shown in Fig. 5. The term $K\lambda/D$ is equal to the value of the intersection of the line with the Y-axis and gives the value of D, while ε is the angular coefficient of the line.

It observed that deformation reduced the crystallite size and microstrain. In the non-aging condition, these reductions were maximum in the CR condition, which obtained a crystallite size and microstrain 62 and 70% smaller than the WD condition, respectively. Increasing the aging time

Table 2 Lattice parameters, phase percentage, microdeformation and crystallite size obtained by Rietveld method and W–H plot for all studied conditions

Time	Phase	*A* (Å)	*B* (Å)	*C* (Å)	%	Microstrain (10^5)	Crystallite (Å)
WD							
0 h	α'	2.8708	2.8708	2.8539	100	286 ± 4	590 ± 22
10 h	α'	2.8667	2.8667	2.8495	90	223 ± 5	328 ± 9
	Ni3(Ti, Mo)	5.0635	4.0538	4.4803	10	···	···
50 h	α'	2.8673	2.8673	2.8535	89	332 ± 25	422 ± 72
	Ni3(Ti, Mo)	5.0645	4.0238	4.4781	11	···	···
200 h	α'	2.8590	2.8590	2.8464	86	180 ± 8	258 ± 9
	Ni3(Ti, Mo)	4.9886	4.0009	4.4490	14	···	···
	Γ	3.5150	3.5150	3.5150	···	···	···
Time	Phase	*A*	*B*	*C*	%	Microstrain	Crystallite
HF							
0 h	α'	2.8595	2.8595	2.8797	100	197 ± 8	245 ± 9
10 h	α'	2.8575	2.8575	2.8710	87	328 ± 8	312 ± 12
	Ni3(Ti, Mo)	5.0538	4.2230	4.4753	13	···	···
50 h	α'	2.8552	2.8552	2.8541	81	529 ± 8	2017 ± 553
	Ni3(Ti, Mo)	5.0688	4.1277	4.4093	19	···	···
	Γ	3.5804	3.5804	3.5804	···	···	···
200 h	α'	2.8659	2.8659	2.8525	89	156 ± 5	228 ± 5
	Ni3(Ti, Mo)	5.1049	4.1606	4.3800	11	···	···
	Γ	3.5899	3.5899	3.5899	···	···	···
Time	Phase	*A*	*B*	*C*	%	Microstrain	Crystallite
CR							
0 h	α'	2.8750	2.8750	2.8603	100	86 ± 6	227 ± 5
10 h	α'	2.8700	2.8700	2.8529	84	116 ± 6	227 ± 5
	Ni3(Ti, Mo)	5.1259	4.1819	4.3748	16	···	···
50 h	α'	2.8641	2.8641	2.8483	81	313 ± 6	581 ± 31
	Ni3(Ti, Mo)	5.1178	4.2240	4.3608	19	···	···
200 h	α'	2.8512	2.8512	2.8664	83	33 ± 7	169 ± 33
	Ni3(Ti, Mo)	5.1225	4.1465	4.3569	17	···	···
	Fe3Mo2	10.926	10.926	19.325	···	···	···

to 10 h increased D and ε values for HF and CR conditions and reduced both values for WD when compared to samples without aging. Increasing the aging time to 50 h both D and ε values increased for all conditions; however with increasing the time to 200 h, it observed a strong decrease in ε and *D*.

Discussion

Maraging steels, after solubilization at 1323 K for 1 h, have a fully martensitic matrix [7]. The diffractogram obtained in the non-aged WD condition showed the peaks (200) and (211) shifted to the right when compared to the α-iron BCC structure, as usually is observed in maraging steels [2, 12, 26–29]. This displacement was possible to be corrected when considering the martensite structure as BCT, as described in recent works [5, 6, 30]. It is believed that the reason for this distortion is the strong supersaturation of the matrix in Ni, Co, Mo and Ti, which, due to their different atomic radius, generate a deformation in the martensite lattice parameter.

With the deformation occurs an increase in dislocation density and the development of a crystallographic texture that depends on the type of deformation applied. In maraging steels, the non-deformed martensite has a preferred orientation (110) [001] and (001) [100] [49]. However, when cold-rolled, a preferential texture occurs in the planes and directions {111} <110> parallel to the normal rolling axis [50]. This change in texture can be verified in the experimental diffractions pattern by the variation of the relative intensity between the peaks, as shown in Fig. 1, where it is

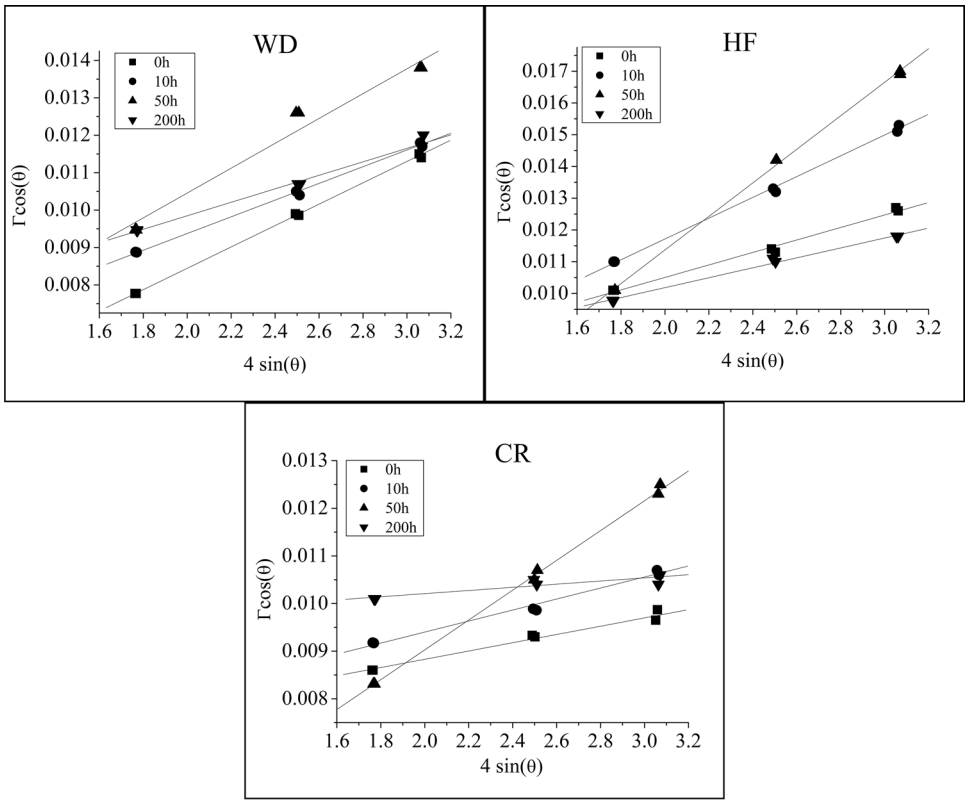

Fig. 5 Plot of Eq 1, W–H equation, used to calculate crystallite size and microstrain for all studied conditions

observed that the relative intensities of the (200) and (211) peaks increased with both HF and CR conditions.

When quantifying crystallite size and microstrain in maraging C250 steels, Mahadevan et al. [51] did not observe linearity in the W–H curve due to the contribution of dislocation in strain widening, characteristic of an anisotropic strain broadening. However, this work verified an isotropic strain broadening, and therefore, the isotropic nature of the crystal is considered. The causes of this divergence probably are: difference of matrix supersaturation between maraging C300 and C250 steels; temperature and cooling rate used in quenching; or even the difference of assuming a cubic or tetragonal matrix when refining the experimental diffractions pattern.

The size of the crystallite tends to reduce with increasing deformation to a saturation point, where deformations from it tend to have little effect on the size of the crystallite [52]. Thus, the application of deformation reduced the size of the crystallite up to 50% when compared with non-deformed samples. However, the HF and CR conditions had a small difference between each other, where the HF had a slightly larger crystallite size due to recrystallization during its hot deformation.

The microstrain is influenced by several factors, between then are: density and dislocation arrangement, variation of grain-to-grain lattice parameters, inclusions, surface relaxation [53] and the existence of coherent, semi-coherent or incoherent precipitates [51]. Thus, separating and quantifying the factors that influence the microstrain in maraging steels, both in the solubilized and in the aged samples, becomes difficult. However, the results verified in non-aged samples show that the value of microstrain reduces significantly with the deformation. The microstrain was, respectively, 31 and 66% lower in the HF and CR conditions than the WD.

When aging all conditions at 773 K for 10 h, the experimental diffraction pattern shows the presence of peaks relative to intermetallic Ni_3(Ti, Mo). These precipitates are metastable, coherent/semi-coherent with the matrix [21] and form in the first few minutes of aging at temperatures above 723 K [16, 40, 54]. The same diffraction pattern is observed in the work of Freitas [44], who also studied a high Ti content maraging C300 steel. However, due to aging at 823 K, the presence of Ni_3(Ti, Mo) observed was smaller and overlapped by reverse austenite peaks.

As consequence of Ni_3(Ti, Mo) precipitation, Ti is almost completely removed from the matrix, followed by Mo [35]. This precipitation occurs preferentially by heterogeneous nucleation in dislocation [21], where the increase in the dislocation density resulted from deformation accelerates precipitation kinetics. Consequently, the CR condition had the larger fraction of precipitates formed, followed by HF and WD conditions, 15, 13 and 10%, respectively.

It is well known that the formation of coherent precipitates leads to an increase in microstrain of the matrix [51]. Thus, the formation of Ni_3(Ti, Mo) together with the microstructure recovery generated an increase in the microstrain under HF and CR conditions. However, the WD condition had a reduction in the microstrain, even in the presence of precipitates, indicating the presence of a third factor acting significantly on microstrain. The matrix supersaturation could be correlated with this factor once the reduction in supersaturation leads to a reduction in distortion in the matrix crystal lattice.

Similarly, precipitate formation, matrix recovery and reduction in supersaturation affected the average crystal size, which behaved in the same way of microstrain.

Rising the aging time to 50 h generates a continuous increase in Ni_3(Ti, Mo) volumetric fraction in all conditions. However, as the tendency of precipitation kinetics is to reduce with a reduction in supersaturation and nucleation site, the increase in Ni_3(Ti, Mo) volumetric fraction was less significant between 10 and 50 h than 0 and 10 h. Increasing aging time also generates austenite in the HF condition, only. That was also verified by Guiza [7] and Freitas [44], which showed that hot forging accelerates the austenite formation.

Although the presence of austenite is an indication of coarsening, dissolution and loss of coherence of precipitate Ni_3(Ti, Mo) with the matrix, it was not possible to verify this result by the crystallite size and/or microstrain, which kept increasing due to the continuous precipitation and recovery of the microstructure under all conditions studied.

For all conditions, the increase in aging time up to 50 h reduced the martensitic matrix tetragonality, and this reduction was maximum in the 50 h aged HF condition where there was a variation of only 0.0012 Å between parameters *a* and *c*. This reduction is consistent with the decrease solid supersaturation due to precipitation and austenite reversion in maraging C300 steels.

After 200 h of aging, the WD condition was the only one that kept an increase in the amount of Ni_3(Ti, Mo) formed. This occurred because, as the precipitation kinetics in these samples were lower than HF and CR, the supersaturation conditions for the precipitate formation remained longer, while in the other conditions, the acceleration of the precipitation kinetics generated by the deformation also accelerated the coarsening and dissolution of these precipitates.

As the dissolution of Ni_3(Ti, Mo) precipitates generates a local increase in Ni and Mo content, after 200 h of aging occurred the formation of reverse austenite diffraction peaks in the WD condition and an increase in those already present in the HF condition, besides the μ phase formation [42] in the CR condition. The dissolution of the precipitates also generated an increase in tetragonal matrix distortion under the HF condition.

Mahadevan et all [51] showed that when a coherent metastable precipitate loses its coherence with coarsening and/or dissolution, misfit dislocation is formed, leading to an apparent reduction in subgrain size and microstrain. Thus, the fast reduction in crystallite size and microstrain observed under all conditions between 50 and 200 h of aging at 773 K shows that occurred an intense destabilization of the Ni_3(Ti, Mo) precipitate, also indicated by the formation of stable phase μ and austenite.

Conclusion

Although the volumetric equilibrium fraction of precipitates makes it difficult to analyze by X-ray diffraction, it was able to verify and quantify the percentage of metastable Ni_3(Ti, Mo) precipitates in a high Ti content maraging C300 steels aged at 773 K.

The martensite structure in the high Ti content C300 maraging steels showed a better fit with the theoretical curves using the tetragonal space group I4. The use of this spatial group also allowed a better adjustment of the W–H curves, which showed good results when calculating microstrain and crystallite size in all studied conditions.

The formation of the Ni_3(Ti, Mo) precipitate together with matrix recovery generates an increase in crystallite size and microstrain. This increase ceases with the loss of coherence and dissolution of these precipitates, when occurs an intense reduction in crystallite size and microstrain to values below that found in non-aged samples.

Both HF and CR conditions show a presence of a distinct texture when compared with WD condition, verified by the significant variation of the relative intensity of the matrix peaks in those conditions.

The deformation, besides increasing the formation kinetics and the maximum volumetric fraction of Ni_3(Ti, Mo), also accelerated the destabilization and dissolution of this precipitate, causing an increase in reverse austenite formation in the HF and μ phase at the CR condition, when compared with WD condition.

Acknowledgements The authors want to acknowledge the CAPES and CNPq for the scholarship and the research grant that allowed the execution of this study.

References

1. J. Tian, M.B. Shahzad, W. Wang, L. Yin, Z. Jiang, Role of Co in formation of Ni–Ti clusters in maraging stainless steel. J. Mater. Sci. Technol. **34**, 1671–1675 (2018). https://doi.org/10.1016/j.jmst.2018.04.020
2. Y. Lian, J. Huang, J. Zhang, C. Zhao, W. Gao, Z. Zhang, M. Ma, Effects of cold rolling on the microstructure and properties

of Fe–Cr–Ni–Mo–Ti maraging steel. Mater. Sci. Eng. A **712**, 663–670 (2018). https://doi.org/10.1016/j.msea.2017.12.041
3. K. Li, L. Wei, B. An, B. Yu, R.D.K. Misra, Aging phenomenon in low lattice-misfit cobalt-free maraging steel: microstructural evolution and strengthening behavior. Mater. Sci. Eng. A **739**, 445–454 (2019). https://doi.org/10.1016/j.msea.2018.10.069
4. C.G. Rajulu, A.G. Krishna, Aging behaviour and tensile strength of maraging. Int. J. Mech. Prod. **8**, 349–356 (2018)
5. T.J.B. Alves, G.C.S. Nunes, L.F.S. Tupan, P.W.C. Sarvezuk, F.F. Ivashita, C.A.S. De Oliveira, A. Paesano, Aging-induced transformations of maraging-400 alloys. Metall. Mater. Trans. A **49**, 3441–3449 (2018). https://doi.org/10.1007/s11661-018-4724-y
6. G.C.S. Nunes, P.W.C. Sarvezuk, T.J.B. Alves, V. Biondo, F.F. Ivashita, A. Paesano Jr, Maraging-350 steel: following the aging through diffractometric, magnetic and hyperfine analysis. J. Magn. Magn. Mater. **421**, 457–461 (2017). https://doi.org/10.1016/j.jmmm.2016.08.052
7. G.M.C. Güiza, C.A.S. Oliveira, Microstructural changes produced by hot forging in a C300 Maraging Steel. Mater. Sci. Eng. A **655**, 142–151 (2016). https://doi.org/10.1016/j.msea.2015.12.084
8. A. Shekhter, H.I. Aaronson, M.K. Miller, S.P. Ringer, E.V. Pereloma, Effect of aging and deformation on the microstructure and properties of Fe–Ni–Ti maraging steel. Metall. Mater. Trans. A **34A**, 973–984 (2004). https://doi.org/10.1007/s11661-004-0024-9
9. A. Ali, M. Ahmed, F.H. Hashmi, A.Q. Khan, Austenite reversion in cold formed 18 wt%Ni 350 grade maraging steel. Mater. Sci. Technol. **10**, 97–101 (1994). https://doi.org/10.1179/mst.1994.10.2.97
10. Y. He, K. Yang, W. Sha, Microstructure and mechanical properties of a 2000 MPa grade co-free maraging steel. Metall. Mater. Trans. A Phys. Metall. Mater. Sci. **36**, 2273–2287 (2005). https://doi.org/10.1007/s11661-005-0100-9
11. F.H. Lang, N. Kenyon, Welding of Maraging Steels, Weld. Res. Concil. (1971) 41
12. F. Tariq, R.A. Baloch, B. Ahmed, N. Naz, Investigation into microstructures of maraging steel 250 weldments and effect of post-weld heat treatments. J. Mater. Eng. Perform. **19**, 264–273 (2009). https://doi.org/10.1007/s11665-009-9455-1
13. A. Shekhter, M.K. Miller, H.I. Aaronson, E.V. Pereloma, S.P. Ringer, Effect of aging and deformation on the microstructure and properties of Fe–Ni–Ti maraging steel. Metall. Mater. Trans. A **35**, 973–983 (2004). https://doi.org/10.1007/s11661-004-1001-z
14. H. Lee, Role of chromium on mechanical properties of Fe–Mn–Ni–Mo–Ti maraging steels. Met. Mater. **1**, 77–83 (1995)
15. G.C.S. Nunes, P.W.C. Sarvezuk, V. Biondo, M.C. Blanco, M.V.S. Nunes, A.M.H. De Andrade, A. Paesano Jr, Structural and magnetic characterization of martensitic Maraging-350 steel. J. Alloys Compd. **646**, 321–325 (2015). https://doi.org/10.1016/j.jallcom.2015.06.008
16. C. Tan, K. Zhou, W. Ma, P. Zhang, M. Liu, T. Kuang, Microstructural evolution, nanoprecipitation behavior and mechanical properties of selective laser melted high-performance grade 300 maraging steel. Mater. Des. **134**, 23–34 (2017). https://doi.org/10.1016/j.matdes.2017.08.026
17. L.V. Tarasenko, V.I. Titov, L.A. Elyutina, Control of variation of properties of maraging chromium-nickel steels in long-term heating. Met. Sci. Heat Treat. **52**, 251–254 (2010). https://doi.org/10.1007/s11041-010-9259-9
18. W. Wang, W. Yan, Q. Duan, Y. Shan, Z. Zhang, K. Yang, Study on fatigue property of a new 2.8 GPa grade maraging steel. Mater. Sci. Eng. A **527**, 3057–3063 (2010). https://doi.org/10.1016/j.msea.2010.02.002
19. H. Kitahara, R. Ueji, N. Tsuji, Y. Minamino, Crystallographic features of lath martensite in low-carbon steel. Acta Mater. **54**, 1279–1288 (2006). https://doi.org/10.1016/j.actamat.2005.11.001
20. E.V. Pereloma, R.A. Stohr, M.K. Miller, S.P. Ringer, Observation of precipitation evolution in Fe–Ni–Mn–Ti–Al maraging steel by atom probe tomography. Metall. Mater. Trans. A **40**, 3069–3075 (2009). https://doi.org/10.1007/s11661-009-9993-z
21. U.K. Viswanathan, G.K. Dey, M.K. Asundi, Precipitation hardening in 350 grade maraging steel. Metall. Trans. A **24**, 2429–2442 (1993). https://doi.org/10.1007/BF02646522
22. U.K. Viswanathan, G.K. Dey, V. Sethumadhavan, Effects of austenite reversion during overageing on the mechanical properties of 18 Ni (350) maraging steel. Mater. Sci. Eng. A **398**, 367–372 (2005). https://doi.org/10.1016/j.msea.2005.03.074
23. W. Sha, Z. Guo, *Maraging Steels: Modelling of Microstructure, Properties and Applications*, 1st edn. (Woodhead Publishing, Oxford, 2009)
24. M. Ahmed, I. Nasim, S.W. Husain, Influence of nickel and molybdenum on the phase stability and mechanical properties of maraging steels. J. Mater. Eng. Perform. **3**, 248–254 (1994). https://doi.org/10.1007/BF02645850
25. X. Li, Z. Yin, Reverted austenite during aging in 18Ni(350) maraging steel. Mater. Lett. **24**, 239–242 (1995). https://doi.org/10.1016/0167-577X(95)00109-3
26. W. Sha, A. Cerezo, G.D.W. Smith, Phase chemistry and precipitation reactions in maraging steels: part II. Co-free T-300 steel. Metall. Trans. A **24**, 1233–1239 (1993). https://doi.org/10.1007/bf02668191
27. M. Cabeza, G. Castro, P. Merino, G. Pena, M. Román, Laser surface melting: a suitable technique to repair damaged surfaces made in 14 Ni (200 grade) maraging steel. Surf. Coat. Technol. **212**, 159–168 (2012). https://doi.org/10.1016/j.surfcoat.2012.09.039
28. P. Venkata Ramana, G. Madhusudhan Reddy, T. Mohandas, Microstructure, hardness and residual stress distribution in maraging steel gas tungsten arc weldments. Sci. Technol. Weld. Join. **13**, 388–394 (2008). https://doi.org/10.1179/174329308x300091
29. M. Masoumi, I.F. De Barros, L. Flavio, G. Herculano, H. Livia, F. Coelho, H. Ferreira, G. De Abreu, Effect of microstructure and crystallographic texture on the Charpy impact test for maraging 300 steel. Mater. Charact. **120**, 203–209 (2016)
30. T.J.B. Alves, G.C.S. Nunes, P.W.C. Sarvezuk, F.F. Ivashita, A.M.H. De Andrade, A. Viegas, A. Paesano, Crystallographic, hyperfine and magnetic characterization of a maraging-400 alloy. Hyperfine Interact. **238**, 1–9 (2017). https://doi.org/10.1007/s10751-017-1418-6
31. F. Zhu, Y.F. Yin, R.G. Faulkner, Microstructural control of maraging steel C300. Mater. Sci. Technol. **27**, 395–405 (2011). https://doi.org/10.1179/026708309X12506933873503
32. W. Sha, Quantification of age hardening in maraging steels and an Ni-base superalloy. Scr. Mater. **42**, 549–553 (2000)
33. Z. Guo, W. Sha, Quantification of precipitation hardening and evolution of precipitates. Mater. Trans. **43**, 1273–1282 (2002). https://doi.org/10.2320/matertrans.43.1273
34. Z. Guo, W. Sha, D. Li, Quantification of phase transformation kinetics of 18 wt% Ni C250 maraging steel. Mater. Sci. Eng. A **373**, 10–20 (2004). https://doi.org/10.1016/j.msea.2004.01.040
35. W. Sha, A. Cerezo, G.D.W. Smith, Phase chemistry and precipitation reactions in maraging steels. Part I. Introduction and study of co-containing C-300 steel. Metall. Trans. A **24**, 1221–1232 (1993). https://doi.org/10.1007/bf02668190
36. S. Floreen, The physical metallurgy maraging steels. Metall. Rev. **13**, 115–128 (1968)
37. H.J. Rack, D. Kalish, The strength and fracture toughness of 18 Ni (350) maraging steel. Matall. Mater. Trans. **2**, 3011–3020 (1971)
38. C. Servant, P. Lacombe, Structural transformations produced during tempering of Fe–Ni–Co–Mo alloys. J. Mater. Sci. **12**, 1807–1826 (1977). https://doi.org/10.1007/BF00566241

39. R. Kapoor, S. Sunil, G. Bharat Reddy, S. Nagaraju, T.S. Kolge, S.K. Sarkar, A. Biswas, A. Sharma, Electric current induced precipitation in maraging steel. Scr. Mater. **154**, 16–19 (2018). https://doi.org/10.1016/j.scriptamat.2018.05.013
40. Y. He, K. Yang, W. Qu, F. Kong, G. Su, Strengthening and toughening of a 2800-MPa grade maraging steel. Mater. Lett. **56**, 763–769 (2002). https://doi.org/10.1016/S0167-577X(02)00610-9
41. V.K. Vasudevan, S.J. Kim, C.M. Wayman, Precipitation reactions and strengthening behavior in 18 Wt Pct nickel maraging steels. Metall. Trans. A Phys. Metall. Mater. Sci. **21A**, 2655–2668 (1990). https://doi.org/10.1007/bf02646061
42. W. Sha, A. Cerezo, G. Smith, Phase chemistry and precipitation reactions in maraging steels: Part IV. Discussion and conclusions. Metall. Trans. A **24**, 1251–1256 (1993). https://doi.org/10.1007/bf02668193
43. J.M. Pardal, S.S.M. Tavares, M.P. Cindra Fonseca, H.F.G. Abreu, J.J.M. Silva, Study of the austenite quantification by X-ray diffraction in the 18Ni-Co-Mo-Ti maraging 300 steel. J. Mater. Sci. **41**, 2301–2307 (2006). https://doi.org/10.1007/s10853-006-7170-y
44. G.H.D.O. Freitas, C.A.S.D. Oliveira, Effect of hot deformation on microstructure, hardness and precipitation kinetics in a C350 maraging steel modified by titanium addition. Mater. Res. (2018). https://doi.org/10.1590/1980-5373-mr-2018-0120
45. H.M. Rietveld, A profile refinement method for nuclear and magnetic structures. J. Appl. Crystallogr. **2**, 65–71 (1969). https://doi.org/10.1107/s0021889869006558
46. A.C. Larson, R.B. von Dreele, *GSAS Manual* (Los Alamos Natl, Lab, 1988)
47. V. Mote, Y. Purushotham, B. Dole, Williamson–Hall analysis in estimation of lattice strain in nanometer-sized ZnO particles. J. Theor. Appl. Phys. **6**, 2–9 (2012). https://doi.org/10.1186/2251-7235-6-6
48. T.J.B. Alves, G.C.S. Nunes, L.F.S. Tupan, P.W.C. Sarvezuk, F.F. Ivashita, C.A.S. De Oliveira, A. Paesano Jr., Aging-induced transformations of maraging-400 alloys. Metall. Mater. Trans. A **49A**, 3441–3449 (2018)
49. V.V. Berezovskaya, S.V. Grachev, F.V. Nineev, D.V. Titorova, V.B. Shirikhin, The role of texture in the processes of aging and delayed fracture of maraging steel. Met. Sci. Heat Treat. **43**, 65–68 (2001)
50. H.F.G. Abreu, S.S.M. Tavares, J.J.M. Silva, J.W.A. Menezes, A.D. Bruno, The influence of an intermediate austenitization heat treatment in the texture of cold-rolled and aged 18% Ni maraging steel. Mater. Charact. **52**, 203–207 (2004). https://doi.org/10.1016/j.matchar.2004.05.007
51. S. Mahadevan, R. Manojkumar, T. Jayakumar, C.R. Das, B.P.C. Rao, Precipitation-induced changes in microstrain and its relation with hardness and tempering parameter in 17-4 PH stainless steel. Metall. Mater. Trans. A Phys. Metall. Mater. Sci. **47**, 3109–3118 (2016). https://doi.org/10.1007/s11661-016-3440-8
52. J. Gubicza, L. Balogh, R.J. Hellmig, Y. Estrin, T. Ungár, Dislocation structure and crystallite size in severely deformed copper by X-ray peak profile analysis. Mater. Sci. Eng. A **400–401**, 334–338 (2005). https://doi.org/10.1016/j.msea.2005.03.042
53. P. Scardi, M. Leoni, Whole powder pattern modelling. Acta Crystallogr. Sect. A Found. Crystallogr. **58**, 190–200 (2002). https://doi.org/10.1107/S0108767301021298
54. J.M. Pardal, S.S.M. Tavares, V.F. Terra, M.R. Da Silva, D.R. Dos Santos, Modeling of precipitation hardening during the aging and overaging of 18Ni–Co–Mo–Ti maraging 300 steel. J. Alloys Compd. **393**, 109–113 (2005). https://doi.org/10.1016/j.jallcom.2004.09.049